



ChemComm

**Towards the Rational Design of Novel Charge-Transfer  
Materials: Biaryls with A Dihedral Angle-Independent Hole  
Delocalization Mechanism**

Journal:	<i>ChemComm</i>
Manuscript ID	CC-COM-03-2018-002595.R1
Article Type:	Communication

SCHOLARONE™  
Manuscripts

## Towards the Rational Design of Novel Charge-Transfer Materials: Biaryls with A Dihedral Angle-Independent Hole Delocalization Mechanism

Received 00th January 20xx,  
Accepted 00th January 20xx

DOI: 10.1039/x0xx00000x

www.rsc.org/

Lena V. Ivanova,<sup>\*a</sup> Tushar S. Navale,<sup>a</sup> Denan Wang,<sup>a</sup> Sergey Lindeman,<sup>a</sup> Maxim V. Ivanov<sup>\*a</sup> and Rajendra Rathore<sup>a,b</sup>

Biaryl cation radicals are important electroactive materials, which show two mechanisms of hole delocalization: static delocalization at small interplanar dihedral angles and dynamic hopping at larger angles, reflecting the interplay between electronic coupling and structural reorganization. Herein, we describe the rational design of biaryls possessing an invariant hole delocalization mechanism.

Biaryls are widely used to explore the fundamental properties of charge transfer in  $\pi$ -conjugated molecular wires.<sup>1-3</sup> For example, in case of a coherent charge transfer without oxidation of the biaryl, the rate of the electron transfer scales as the square of the electronic coupling. However, at the steady-state condition that involves complete oxidation of the biaryl, two scenarios are possible:<sup>4-6</sup> the hole can be (statically) delocalized over both aryls, or can (dynamically) hop between them. The favored mechanism depends on the interplay between electronic coupling ( $H_{ab}$ ), determined by orbital overlap, and reorganization energy ( $\lambda$ ), which involves slow modes of solvent reorientation and fast bond vibrations associated with charge transfer.<sup>7</sup> As the charge transfer in the long molecular wires is often dominated by an incoherent hopping mechanism,<sup>8-11</sup> rational design of molecular assemblies exhibiting hole delocalization via (steady-state) dynamic hopping is of particular importance.

A recent study of a set of biaryl cation radicals based on the 1,2-dimethoxy aryl (i.e., veratrole) groups with varied number of methylenes in the linker ( $Vn$ ,  $n = 1-6$ , Fig. 1A, Chart S1 in the ESI) showed that the hole is statically delocalized for interplanar dihedral angles ( $\varphi$ ) in the  $0^\circ$ - $45^\circ$  range and dynamically hops in biaryls with larger angles.<sup>4</sup> Building on this work, in the context of a rational design of materials for long-range charge transfer we ask, *can one design a model biaryl*

where dynamic hopping occurs even for the smallest interplanar dihedral angles?

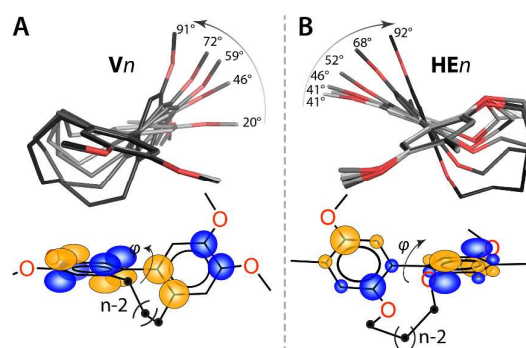


Fig. 1 Superimposed structures and schematic representation of HOMO of biaryls with varied length of  $n$ -methylene linker and aryl groups based on (A) veratrole and (B) hydroquinone ether moieties.

In  $Vn$  series the favorable nodal arrangement of HOMO promotes efficient orbital overlap (Fig. 1A) and large electronic coupling that is reflected in the extensive hole delocalization up to  $\varphi = 45^\circ$ . Moving the methoxy groups from 1,2 to 2,5 positions alters the arrangement of HOMO lobes,<sup>12,13</sup> and is expected to reduce the orbital overlap and lead to a dynamic hopping mechanism even at smaller interplanar angles. In this communication we will show that in biaryls based on hydroquinone ether with  $n$ -methylene linker ( $HEn$ ,  $n = 1-6$ , Fig. 1B, Chart S1 in the ESI), the dynamic hopping mechanism begins from  $HE1^{+\bullet}$  ( $\varphi = 24^\circ$ ), as opposed to  $Vn$  series where the switchover occurs for  $V4^{+\bullet}$  ( $\varphi = 45^\circ$ ). Such a contrasting angular dependence of the hole delocalization mechanism in two similar biaryls underscores an importance of the analysis of the frontier molecular orbitals in the rational design of novel charge-transfer materials, where the mechanism of hole delocalization can be tailored to achieve desired charge-transfer characteristics.

Compounds  $HE1$ - $HE6$  were synthesized following literature procedures<sup>14, 15</sup> and characterized by  $^1H/^{13}C$  NMR and MALDI spectroscopies and X-ray crystallography of representative molecules (see ESI for full details). Crystal structures of neutral

<sup>a</sup> Department of Chemistry, Marquette University, P.O. Box 1881, Milwaukee, WI 53201-1881, USA. E-mail: maxim.ivanov@protonmail.com, lenuel.ivanova@gmail.com

<sup>b</sup> Deceased February 16, 2018

† Footnotes relating to the title and/or authors should appear here.

Electronic Supplementary Information (ESI) available: Full experimental details for  $HEn$ , where  $n=1-6$ , and computational details. For ESI and crystallographic data in CIF or other electronic format see DOI: 10.1039/x0xx00000x

**HE $n$**  showed that the interplanar dihedral angles between two aryl groups lie in the 41°–92° range (Fig. 2). Unfortunately, repeated attempts to isolate crystal structure of **HE $n$ <sup>••</sup>** were unsuccessful.

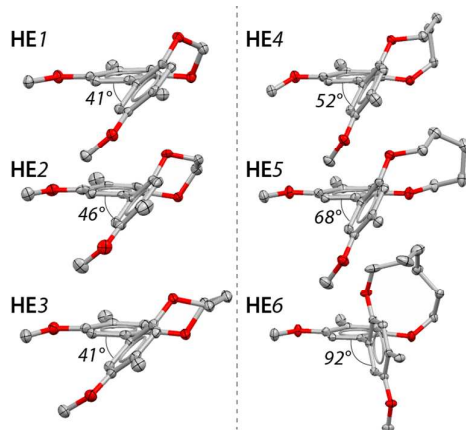


Fig. 2 ORTEP diagrams (50% probability) of **HE $n$** . Hydrogens are omitted for clarity.

Compounds **HE $n$**  showed reversible cyclic voltammograms (CVs), with an oxidation potential that varied within 200 mV (Fig. 3A), in contrast to the 470 mV range observed for the **V $n$**  series. Furthermore, oxidation potentials ( $E_{ox}$ ) of **HE $n$**  decrease with increasing number of methylenes going from  $E_{ox} = 0.82$  V (**HE1**,  $\phi = 41^\circ$ ) to 0.68 V vs Fc/Fc<sup>+</sup> (**HE4**,  $\phi = 52^\circ$ ), and remain invariant up to **HE5** and **HE6** (0.62 and 0.63 V vs Fc/Fc<sup>+</sup>, respectively), although the dihedral angle  $\phi$  continues to increase ( $\phi = 68^\circ$  and  $92^\circ$ , respectively). This is in sharp contrast with the evolution of  $E_{ox}$  in **V $n$**  series, where increasing the number of methylenes leads to an increase in the  $E_{ox}$  due to the decreasing interchromophoric electronic coupling (Table S3 in the ESI).<sup>4</sup>

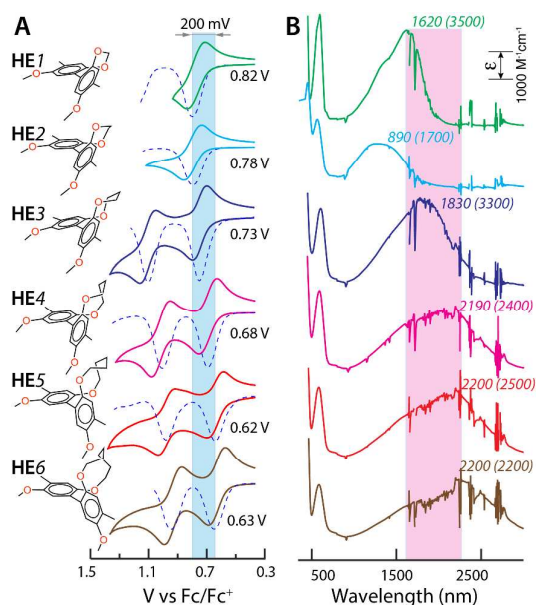


Fig. 3 (A) Cyclic voltammograms (CVs) and indicated  $E_{ox}$  of 2 mM **HE1**–**HE6** in  $\text{CH}_2\text{Cl}_2$  (0.1 M *n*-Bu<sub>4</sub>NPF<sub>6</sub>) at a scan rate of 200 mV s<sup>-1</sup> and 22°C. (B) Absorption spectra of **HE1<sup>••</sup>**

**HE6<sup>••</sup>** in  $\text{CH}_2\text{Cl}_2$  at 22°C. The positions (nm) of the lowest-energy band with molar absorptivity ( $\text{M}^{-1}\text{cm}^{-1}$ ) in parenthesis are indicated.

The electrochemical stability of **HE $n$**  prompted us to generate their cation radicals via quantitative<sup>16</sup> redox titrations using robust aromatic oxidants<sup>17</sup> (see ESI for details). The cation radicals exhibit a characteristic near-IR band (Fig. 3B), which shifts red from 1620 nm in the absorption spectra of **HE1<sup>••</sup>**, **HE3<sup>••</sup>** and **HE4<sup>••</sup>**, accompanied by a minor reduction in molar absorptivity from 3500 to 2400  $\text{M}^{-1}\text{cm}^{-1}$ . Importantly, the position of the near-IR band remains invariant in **HE4<sup>••</sup>**–**HE6<sup>••</sup>**, appearing at 2190, 2200, and 2200 nm, respectively, with similar molar absorptivities of 2400, 2500, 2200  $\text{M}^{-1}\text{cm}^{-1}$ , respectively. Surprisingly, the near-IR band in the spectrum of **HE2<sup>••</sup>** demonstrated an unusual blue shift to 890 nm and a reduction in molar absorptivity (1700  $\text{M}^{-1}\text{cm}^{-1}$ ). We compare these findings to the **V $n$ <sup>••</sup>** series, where the near-IR band shifts by some 1000 nm from 1098 to 2050 nm with the intensity of the band dramatically decreasing by some 10,000  $\text{M}^{-1}\text{cm}^{-1}$  (Table S3 in the ESI).<sup>4</sup>

In order to rationalize the disparate evolution with increasing  $n$  of the redox and optical properties of **HE $n$**  and **V $n$** , we carried out DFT calculations using a customized B1LYP-40 functional that has been parameterized to accurately reproduce the electronic structure of  $\pi$ -conjugated cation radicals.<sup>18,19</sup> The DFT calculations at B1LYP-40/6-31G(d)+PCM( $\text{CH}_2\text{Cl}_2$ ) level of theory well reproduced the available X-ray structures of neutral **HE $n$** , and showed that upon oxidation, the interplanar dihedral angle decreases, with the most pronounced changes corresponding to the biaryls with a longer methylene linker (Table S4 in the ESI). The resulting equilibrium dihedral angles of the optimized **HE $n$ <sup>••</sup>** span a very narrow range of values ( $\phi_{CR} = 24^\circ$ – $49^\circ$ , Fig. 4A).

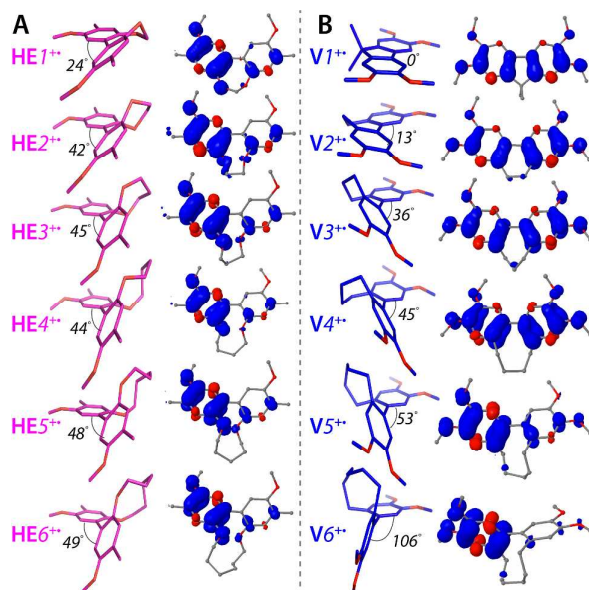


Fig. 4 Calculated structures and spin-density plots of (A) **HE $n$ <sup>••</sup>** and (B) **V $n$ <sup>••</sup>** series.

Analysis of the calculated bond length changes in **HE $n$ →HE $n$ <sup>••</sup>** transformations showed that the oxidation-

induced structural reorganization follows a quinoidal distortion of each aromatic ring (Table S7 in the ESI). Importantly, the distribution of the structural reorganization is uneven with most of the reorganization localized on a single aryl group for all  $\text{HE}n^{**}$ . The natural population analysis (NPA)<sup>20</sup> of the charge density in  $\text{HE}n^{**}$  further confirmed that most (i.e., 0.9/0.8) of the spin/charge is localized on the same aryl (Table S8 in the ESI), which can be visually seen from the spin-density plots of  $\text{HE}n^{**}$  (Fig. 4A).

In contrast, the  $\text{V}n^{**}$  series displays a mechanism of hole delocalization that is extremely sensitive to the value of the interplanar dihedral angle (Fig. 4B).<sup>4</sup> Starting from planar  $\text{V}1^{**}$ , where the hole is statically delocalized over both aryl groups, increasing the interplanar angle changes the mechanism of hole distribution to the dynamic hopping, as evidenced by the change in the slopes of the oxidation potentials ( $E_{\text{ox}}$ ) and cation radical excitation energies ( $\nu_{\text{max}}$ ) against  $\cos(\varphi_{\text{CR}})$  as shown in Figs. 5A and 5B, respectively.

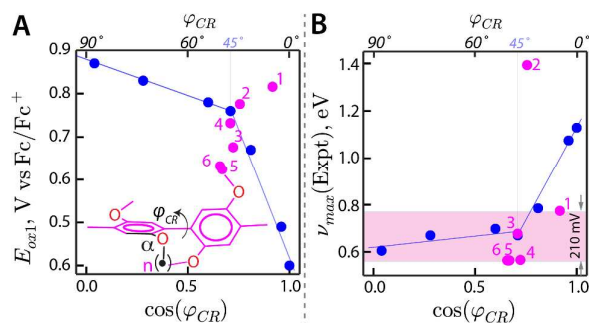


Fig. 5 Plots of experimental (A)  $E_{\text{ox}1}$  and (B)  $\nu_{\text{max}}$  against  $\cos(\varphi_{\text{CR}})$  for  $\text{HE}n$  (magenta) and  $\text{V}n$  (blue).

The contrasting evolution in the mechanism of hole delocalization with respect to the varied interplanar angle in  $\text{V}n^{**}$  and  $\text{HE}n^{**}$  must arise from differences in electronic coupling ( $H_{ab}$ ) and structural reorganization ( $\lambda$ ) parameters. According to the Marcus-Hush theory, the characteristic interplanar dihedral angle at which the mechanism of hole delocalization changes corresponds to the case where  $2H_{ab} = \lambda$ . This fact implies that in  $\text{HE}n^{**}$  series, the electronic coupling must be less than the half of the reorganization energy ( $H_{ab} < \lambda/2$ ). Indeed, molecular orbital analysis showed that the electronic coupling in  $\text{HE}n$  lies in the 0.1–0.3 eV range (Fig. S9 in the ESI), while TD-DFT calculations showed<sup>21</sup> that the reorganization energy is significantly higher, 0.8–1.2 eV (Table S4 in the ESI), and therefore both parameters satisfy the  $H_{ab} < \lambda/2$  criteria. The dynamic hole hopping in  $\text{HE}n^{**}$  is estimated to occur on the picosecond timescale as estimated by the Marcus equation<sup>22</sup> (Table S9 in the ESI).

The dynamic hole hopping mechanism evidenced in  $\text{HE}n^{**}$  should lead to a near-invariance of  $E_{\text{ox}}$  with interplanar angle, comparable to the modest  $\sim 110$  mV increase of  $E_{\text{ox}}$  in  $\text{V}n$  series for  $\varphi_{\text{CR}} = 45^\circ$ – $90^\circ$ . However, electrochemical analysis of  $\text{HE}n$  showed that  $E_{\text{ox}}$  decreases by 200 mV over a significantly smaller range of interplanar angles ( $\varphi_{\text{CR}} = 24^\circ$ – $49^\circ$ ). A further analysis of the X-ray structures of  $\text{HE}n$  and calculated

equilibrium structures of  $\text{HE}n^{**}$  revealed that the aryl groups are not equivalent across the series, as the varied length of the methylene linker changes the orientation of the ether group with respect to aromatic plane. For example, upon incorporation of additional methylenes, the dihedral angle C–O–C<sub>ar</sub>–C<sub>ar</sub> varies in the  $\alpha_{1/2} = 180^\circ$ – $2^\circ$  range (Table S4 in the ESI).

It has been established that orientation of the methoxy groups relative to the aromatic plane in various  $\text{HE}$  derivatives has a dramatic impact on their oxidation potentials.<sup>23</sup> For example, a computational relaxed potential scan of a model 2,5-dimethoxy-*p*-xylene ( $\text{DMX}$ ), where dihedral angle C–O–C<sub>ar</sub>–C<sub>ar</sub> is varied from completely planar ( $\alpha = 0^\circ$ ) to a perpendicular ( $\alpha = 90^\circ$ ) arrangement, showed that the relative energy of  $\text{DMX}^{**}$  dramatically increases by 0.4 eV (Fig. S13 in the ESI). Thus, when the number of methylenes in the linker of  $\text{HE}n$  is small, the orientation of the ether groups is forced to adopt a more energetically demanding out-of-plane arrangement, leading to higher oxidation potentials. Upon addition of more methylenes, the linker flexibility increases and the ether groups can adopt a more energetically favorable in-plane arrangement, lowering the oxidation potential.

In hindsight, the choice of linking two aryl groups via a methylene bridge involving the ether group is not ideal, as the reorganization energy and electronic coupling parameters may be influenced by the linker in an unpredictable manner. For example, compound  $\text{HE}2$  is an outlier in the electronic absorption spectra of  $\text{HE}n^{**}$  series, with its spectrum displaying a blue-shifted absorption band in contrast with the general trend of the absorption band shifting to the longer wavelengths (Fig. 3). An improved series of  $\text{HE}$ -based biaryls would have ether groups that are rigidly held in the aromatic plane by additional ethylene bridges (i.e.,  $\text{pHE}n$ , Fig. 6A). Indeed, preliminary calculations show that hole is largely localized on a single aryl group in the entire  $\text{pHE}n^{**}$  series as in  $\text{HE}n^{**}$  series, yet their oxidation potentials and cation radical excitation energies are weakly dependent on the interplanar dihedral angle  $\varphi$  and show the expected weak increase with increasing  $\varphi$  (Fig. 6B).

We have demonstrated a rational approach to the design of novel charge-transfer molecular assemblies in which one simultaneously considers both geometrical and electronic structure properties on the example of model biaryls ( $\text{V}n$ ,  $\text{HE}n$  and  $\text{pHE}n$  series). In  $\text{V}n^{**}$  two mechanisms of hole distribution exist that depend on the value of the interplanar dihedral angle, i.e. static delocalization when  $\varphi \leq 45^\circ$  and dynamic hopping when  $\varphi > 45^\circ$ . A modification in position of methoxy groups from  $\text{V}n$  to  $\text{HE}n$  changes the nodal arrangement of HOMO and reduces the orbital overlap at the biaryl linkage, resulting in the dynamic hopping mechanism starting from  $n = 1$ , i.e.,  $\text{HE}1^{**}$ . One may further refine the biaryl structure by forcing the orientation of the ether groups into the aromatic plane via additional methylene bridges (i.e.,  $\text{pHE}n$ ) in order to achieve a near-invariance of the oxidation potentials and cation radical excitation energies with respect to the interplanar dihedral angle. This work thus highlights the importance of frontier molecular orbital analysis for the

rational design of novel long-range charge-transfer materials with tailored redox and optoelectronic properties.

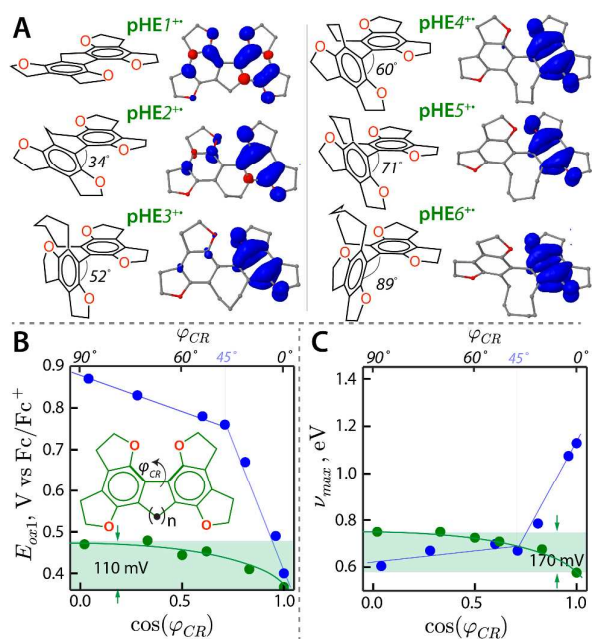


**Fig. 6** (A) Structures and spin density plots of pHE n+•. Plots of (B)  $E_{ox1}$  and (C)  $V_{max}$  of  $V_n$  (blue) and pHE n (green) against  $\cos(\varphi_{CR})$ . Values for  $V_n$  are experimental, while values for pHE n were obtained using DFT and scaled to experimental data using the linear correlation in Fig. S14.

We thank the NSF (CHE-1508677) and NIH (R01-HL112639-04) for financial support, and Prof. Scott Reid for helpful discussions. The calculations were performed on the high-performance computing cluster Pèrè at Marquette University and XSEDE.

## Conflicts of interest

There are no conflicts to declare.

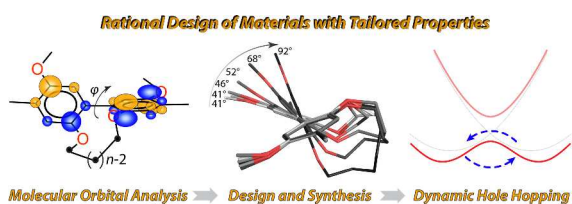
## Notes and references

‡ Crystal structure data for HE1 [C<sub>17</sub>H<sub>18</sub>O<sub>4</sub>] (raj10f): FW = 286.31, C2/c, a = 11.1202(3) Å, b = 11.2585(3) Å, c = 11.2577(3) Å,  $\alpha = 90$ ,  $\beta = 99.472(2)$ ,  $\gamma = 90$ , Z = 4, V = 1390.21(6) Å<sup>3</sup>, D = 1.368 g cm<sup>-3</sup>, T = 100 K, 1202 reflections measured, 1126 unique reflections,  $R_{int} = 0.0220$ , 133 parameters refined, R(all) = 0.0291, wR(all) = 0.0778, S = 0.980 (CCDC 1830466). Crystal structure data for HE2 [C<sub>18</sub>H<sub>20</sub>O<sub>4</sub>] (raj10d): FW = 286.31, Pca21, a = 48.377(2) Å, b = 7.5624(3) Å, c = 21.0775(10) Å,  $\alpha = 90$ ,  $\beta = 90$ ,  $\gamma = 90$ , Z = 4, V = 7711.2(6) Å<sup>3</sup>, D = 1.294 g cm<sup>-3</sup>, T = 100 K, 13208 reflections measured, 12390 unique reflections,  $R_{int} = 0.0334$ , 1013 parameters refined, R(all) = 0.0573, wR(all) = 0.1411, S = 1.019 (CCDC 1830465). Crystal structure data for HE3 [C<sub>19</sub>H<sub>22</sub>O<sub>4</sub>] (raj10m): FW = 314.37, Pbcn, a = 7.4984(2) Å, b = 10.1051(2) Å, c = 20.5483(4) Å,  $\alpha = 90$ ,  $\beta = 90$ ,  $\gamma = 90$ , Z = 4, V = 1556.99(5) Å<sup>3</sup>, D = 1.341 g cm<sup>-3</sup>, T = 100 K, 1365 reflections measured, 1303 unique reflections,  $R_{int} = 0.0206$ , 150 parameters refined, R(all) = 0.0295, wR(all) = 0.0846, S = 0.976 (CCDC 1830463). Crystal structure data for HE4 [C<sub>20</sub>H<sub>24</sub>O<sub>4</sub>] (raj0z): FW = 328.39, C2/c, a = 40.9654(10) Å, b = 8.6677(2) Å, c = 9.9042(2) Å,  $\alpha = 90$ ,  $\beta = 102.185(1)$ ,  $\gamma = 90$ , Z = 8, V = 3437.51(13) Å<sup>3</sup>, D = 1.269 g cm<sup>-3</sup>, T =

100 K, 2948 reflections measured, 2654 unique reflections,  $R_{int} = 0.0217$ , 222 parameters refined, R(all) = 0.0395, wR(all) = 0.0861, S = 1.018 (CCDC 1830467). Crystal structure data for HE5 [C<sub>21</sub>H<sub>26</sub>O<sub>4</sub>] (raj10j): FW = 342.42, P-1, a = 10.9041(3) Å, b = 11.8130(3) Å, c = 15.3920(4) Å,  $\alpha = 67.718(1)$ ,  $\beta = 79.863(1)$ ,  $\gamma = 89.142(1)$ , Z = 4, V = 1803.04(8) Å<sup>3</sup>, D = 1.261 g cm<sup>-3</sup>, T = 100 K, 5910 reflections measured, 5574 unique reflections,  $R_{int} = 0.0143$ , 460 parameters refined, R(all) = 0.0332, wR(all) = 0.0868, S = 1.006 (CCDC 1830464). Crystal structure data for HE6 [C<sub>22</sub>H<sub>28</sub>O<sub>4</sub>] (raj10i): FW = 356.44, P65, a = 9.0951(1) Å, b = 9.0951(1) Å, c = 38.8243(9) Å,  $\alpha = 90$ ,  $\beta = 90$ ,  $\gamma = 120$ , Z = 6, V = 2781.31(8) Å<sup>3</sup>, D = 1.277 g cm<sup>-3</sup>, T = 100 K, 2722 reflections measured, 2718 unique reflections,  $R_{int} = 0.0162$ , 249 parameters refined, R(all) = 0.0274, wR(all) = 0.2722, S = 1.016 (CCDC 1830462).

- 1 D. M. Guldi, H. Nishihara and L. Venkataraman, *Chem. Soc. Rev.*, 2015, **44**, 842.
- 2 L. Venkataraman, J. E. Klare, C. Nuckolls, M. S. Hybertsen and M. L. Steigerwald, *Nature.*, 2006, **442**, 904.
- 3 D. Vonlanthen, A. Mishchenko, M. Elbing, M. Neuburger, T. Wandlowski and M. Mayor, *Angew. Chem. Int. Ed.*, 2009, **48**, 8886.
- 4 M. R. Talipov, T. S. Navale, M. M. Hossain, R. Shukla, M. V. Ivanov and R. Rathore, *Angew. Chem. Int. Ed.*, 2017, **129**, 272.
- 5 A. Heckmann and C. Lambert, *Angew. Chem. Int. Ed. Engl.*, 2012, **51**, 326.
- 6 J. Hankache and O. S. Wenger, *Chem. Rev.*, 2011, **111**, 5138.
- 7 B. S. Brunschwig, C. Creutz and N. Sutin, *Chem. Soc. Rev.*, 2002, **31**, 168.
- 8 C. E. Smith, S. O. Odoh, S. Ghosh, L. Gagliardi, C. J. Cramer and C. D. Frisbie, *J. Am. Chem. Soc.*, 2015, **137**, 15732.
- 9 G. Li, N. Govind, M. A. Ratner, C. J. Cramer and L. Gagliardi, *J. Phys. Chem. Lett.*, 2015, **6**, 4889.
- 10 C. Lambert, G. Nöll and J. Schelter, *Nat. Mater.*, 2002, **1**, 69.
- 11 M. E. Walther and O. S. Wenger, *Chemphyschem.*, 2009, **10**, 1203.
- 12 M. R. Talipov, T. S. Navale and R. Rathore, *Angew. Chem. Int. Ed. Engl.*, 2015, **54**, 14468.
- 13 M. V. Ivanov, V. J. Chebny, M. R. Talipov and R. Rathore, *J. Am. Chem. Soc.*, 2017, **139**, 4334.
- 14 R. Rathore and J. K. Kochi, *J. Org. Chem.*, 1995, **60**, 7479.
- 15 L. Zhai, R. Shukla and R. Rathore, *Org. Lett.*, 2009, **11**, 3474.
- 16 M. R. Talipov, A. Boddeda, M. M. Hossain and R. Rathore, *J. Phys. Org. Chem.*, 2015, **29**, 227.
- 17 M. R. Talipov, R. Rathore, *Organic Redox Systems: Synthesis, Properties, and Applications*, John Wiley & Sons, Hoboken, NJ, 2015.
- 18 M. R. Talipov, A. Boddeda, Q. K. Timerghazin and R. Rathore, *J. Phys. Chem. C*, 2014, **118**, 21400.
- 19 M. V. Ivanov, M. R. Talipov, T. S. Navale and R. Rathore, *J. Phys. Chem. C*, 2018, **122**, 2539.
- 20 A. E. Reed, R. B. Weinstock and F. Weinhold, *J. Chem. Phys.*, 1985, **83**, 735.
- 21 Note that in the case of dynamic hopping mechanism excitation energy of the biaryl cation radical equals reorganization energy  $\lambda$ , see ref. 7.
- 22 R. A. Marcus and N. Sutin, *Biochim. Biophys. Acta.*, 1985, **811**, 265.
- 23 M. V. Ivanov, D. Wang, S. H. Wadumethridge and R. Rathore, *J. Phys. Chem. Lett.*, 2017, **8**, 4226.

TOC:



Sentence highlighting the novelty of the work:

Herein, we demonstrate a rational design of novel materials using FMO analysis on the example of biaryls possessing an interplanar dihedral angle-invariant mechanism of hole delocalization.